Regional Frequency Stability Constrained Resilience Enhancement Strategies for Distribution Systems with Flexible Energy Resources

YANG Hongkun
Key Laboratory of Control of Power Transmission and Conversion
Shanghai Jiao Tong University
Shanghai, China
yanghongkun@sjtu.edu.cn

WANG Xu
Key Laboratory of Control of Power Transmission and Conversion
Shanghai Jiao Tong University
Shanghai, China
wangxu1989@sjtu.edu.cn

JIANG Chuanwen
Key Laboratory of Control of Power Transmission and Conversion
Shanghai Jiao Tong University
Shanghai, China
jiangcw@sjtu.edu.cn

WANG Yushan
Substation Transportation Inspection Center
State Grid Chongqing Electric Power Company
Chongqing, China
896670390@qq.com

CHEN Qizhen
Key Laboratory of Control of Power Transmission and Conversion
Shanghai Jiao Tong University
Shanghai, China
drivingeyes@sjtu.edu.cn

WU Hanxiao
Key Laboratory of Control of Power Transmission and Conversion
Shanghai Jiao Tong University
Shanghai, China
1362257580@qq.com

2024 IEEE/IAS Industrial and Commercial Power System Asia (I&CPS Asia) | 979-8-3503-5229-0/24/$31.00 ©2024 IEEE | DOI: 10.1109/ICPSASIA61913.2024.10761452

***Abstract*—Extreme weather can easily trigger emergency faults in distribution networks, which in turn can have a significant impact on the frequency within the region, compromising the stable and reliable operation of the power grid during disasters. Traditional resilient distribution networks' flexible energy resource (FERs) allocation and scheduling strategies primarily focus on the steady-state operation before and after faults, with little consideration for the impact of unbalanced currents on regional frequency during the dynamic process when lines are disconnected, leading to potential frequency violations. this paper proposes a resilience enhancement strategy for distribution network systems with FERs that incorporates regional frequency stability constraints. With the dual objectives of optimizing resilience enhancement and minimizing economic costs, the distribution network system is strategically employed to regulate the mobility scheduling of FERs, thus establishing a comprehensive resilience enhancement model. By harnessing the capabilities of numerical simulation techniques, a linear representation of the Rate of Change of Frequency (ROCOF) and the frequency nadir in regions affected by faults is achieved, which significantly reduces the complexity of model resolution and aids in the formulation of a resilience enhancement strategy for distribution network flexible resources, taking into account constraints associated with regional frequency stability. The efficacy of the proposed method is corroborated through its application to the IEEE 33-node distribution network system.**

Keywords—resilience enhancement, flexible energy resources, Mobile Energy Storage Systems, frequency constrain

I. INTRODUCTION

In recent years, the threat posed to electrical safety by extreme weather and climate-related events has become more pronounced. In September 2022, Typhoon "Muifa" caused a total of 65 lines tripping down in Shanghai, significantly impacting the distribution networks in coastal areas[1]. In September 2023, Typhoon "Soudelor" along with extreme windstorms and heavy rains severely disrupted the power systems in most parts of southern China[2]. Over the next few decades, as the effects of global warming, it is anticipated that the likelihood of encountering various risks triggered by climate change will increase further. There is an urgent need to pay attention to the potential impacts and long-term risks of climate change on the safety of grids. As the proportion of FERs in power systems continues to increase, how to fully leverage the regulatory capabilities of FERs, enhance the operational stability and reliability of power systems under extreme weather conditions, and strengthen their resilience to reduce customer outage losses has become a focus of current research.

Reference [3] employs an optimal recovery strategy that leverages the coordinated action of microgrids, distributed generation facilities, and additional resources to restore essential loads. A strategy to enhance resilience in distribution networks during typhoon conditions, incorporating both hierarchical load shedding and peer-level load reduction, was proposed based on the modeling of typhoon storms in [4]. In [5],a network reconfiguration and fault repair optimization method aimed at rapid recovery of distribution networks against extreme disasters was proposed, based on a resilience representation model using mechanical mapping and a dynamic interactive optimization framework. Reference [6] proposes a two-stage power restoration strategy that includes FERs such as electric vehicles, mobile storage, and emergency warehouses for repair crews. A resilience-driven dispatch method for MPSs and RCs was proposed in [7], employing a hierarchical multi-agent reinforcement learning technique implemented within a dual-layer framework, constructed through mixed decisions.

979-8-3503-5229-0/24/$31.00 @2024 IEEE

Under extreme weather conditions, power system faults are likely to result in system frequency exceeding its limits. Fortunately, it was derived and proven that regional frequency constraints could be represented linearly, and the samples obtained from dynamic simulations of the power system were acquired using linear regression methods in [8] and [9]. In proposing a novel unit scheduling strategy, [10] considered the dynamic differences in frequency across regions, as well as the frequency response characteristics of wind and photovoltaic power generation, ensuring frequency safety and stability across interconnected systems in multiple regions under highly uncertain conditions. In [11], the proposal highlighted that isolated microgrids could face scenarios where frequency constraints are not satisfied, especially under significant power imbalance conditions. While [12] succeeded in establishing an operational model incorporating transient safety constraints, the model still presents considerable challenges in terms of solvability.Reference [13] takes into account the system's frequency response reserves in the preventive scheduling of distribution networks, aiming to constrain the steady-state frequency deviation that occurs during the formation of microgrids.

Most strategies for enhancing the resilience of FERs overlook the impact of unbalanced currents caused by power system line faults on regional frequency stability. Some methods that consider frequency variations under faults also lack good scalability. This paper proposes a resilience enhancement strategy for distribution network systems with FERs that incorporates regional frequency stability constraints. With the objective of optimizing resilience enhancement and minimizing economic costs, the grid-connected distribution network system is utilized to constrain the mobility scheduling of FERs, thereby establishing a resilience enhancement model with configured FERs. Utilizing numerical simulation techniques enables the attainment of a linear representation of the ROCOF and the frequency nadir in the fault-affected regions, thereby simplifying the complexity of model resolution and facilitating the development of a resilience enhancement strategy for flexible resources in distribution networks, which incorporates constraints related to regional frequency stability. The proposed method's effectiveness is validated through experiments conducted on the IEEE 33-node distribution network system.

II. DERs Support for Resilience Enhancement Strategy

Currently, the mainstream approach to resilience assessment is refined through three phases: pre-disaster prevention, mid-disaster response, and post-disaster recovery. Considering that this study examines the influence of FERs on support capabilities under extreme weather conditions. It defines the resilience index of the power distribution network as the total load shedding loss experienced. As illustrated in Fig. 1 and (1), the enclosed area between the two load curves represents the cumulative load shedding volume R [14].

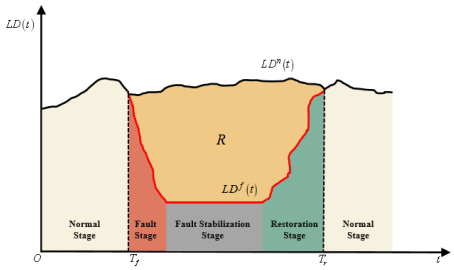

Fig. 1. Resilience assessment diagram

$$R = \int_{T_f}^{T_r} \sum_{i=1}^{N} c_i^{cut} \left(LD_i^n(t) - LD_i^f(t) \right) dt \tag{1}$$

T_f and T_r denote the commencement and cessation times of typhoon conditions faced by the power distribution network, respectively. c_i^{cut} represents the cost associated with load shedding. $LD_{i,n}(t)$ and $LD_{i,f}(t)$ signify the normal and affected load levels of the power distribution network when it is not under the influence of a typhoon and when it is impacted by a typhoon, respectively.A lower value of R indicates a higher level of resilience in the power distribution network, demonstrating a stronger support capability of FERs for the system's power supply. To comprehensively consider the actual support needs of various types of loads in the distribution network, the loads are classified into three categories: (1) non-sheddable loads; (2) critical loads; and (3) non-critical loads, distinguished by the magnitude of load shedding costs.

Distributed generators (DGs) and MESSs, as key FERs within the power grid, play an essential role in enhancing grid resilience. This paper through the optimization of the operational behaviors of DGs and the charging, discharging, and transportation activities of MESSs, aims to minimize the grid resilience index R and the operational costs of MESSs. It proposes a resilience enhancement model for dealing with distribution network line failures under extreme weather conditions, intending to effectively improve the grid's capability to respond to emergencies through precise scheduling.

A. The Objective Function

Given the imperative role of grid operators in addressing power line failures and ensuring electricity supply under extreme weather conditions, this paper adopts the perspective of grid operators. It focuses on mitigating the impact of power supply interruptions during disasters through the strategic deployment of MESSs, without considering the generation costs of DGs and the charging/discharging costs of MESSs. By strategically planning the allocation of MESSs, the paper aims to achieve an optimal balance between enhancing grid resilience and the scale of MESS deployment. Consequently, the objective function F is constructed as follows:

$$\begin{aligned} &\min F = F_{load} + F_{MESS} \\ &F_{load} = \sum_{t=T_f}^{T_r} \sum_{i=1}^{N} c_i^{cut} \left(LD_{i,t}^n - LD_{i,t}^f \right) \\ &F_{MESS} = \sum_{i=1}^{N_m} \frac{c_{MESS} E_i^{MESS}}{k} \end{aligned} \tag{2}$$

Where, F_{load} and F_{MESS} denote the costs associated with load shedding and the deployment of MESSs, respectively. c_{MESS} denotes the cost per unit of MESS, and k denotes the average number of times the MESSs is utilized over its lifespan to respond to extreme events.

B. Steady-state Constraints

Steady-state constraints primarily consider energy balance on an hourly scale, including the steady-state parameter constraints of each device.

1) DGs constrains:

$$P_{\min}^{DG} \le P_{i,t}^{DG} \le P_{\max}^{DG} \tag{3}$$

$$R_{down} \le P_{i,t+1}^{DG} - P_{i,t}^{DG} \le R_{up} \tag{4}$$

$P_{\min}^{DG}$ and $P_{\max}^{DG}$ denote the upper and lower output limits of DGs respectively, while R_{down} and R_{up} denote the upper and lower bounds of DGs' ramping capabilities.

2) MESSs constrains:

$$\begin{cases} 0 \le P_{i,t}^{ch} \le \xi_{i,t}^{ch} P_{\max}^{ch} \\ 0 \le P_{i,t}^{dis} \le \xi_{i,t}^{dis} P_{\max}^{dis} \\ \xi_{i,t}^{ch} + \xi_{i,t}^{dis} \le 1 \end{cases} \tag{5}$$

Equation (5) denotes the charging and discharging power constraints of MESSs, where $P_{\max}^{ch}$ and $P_{\max}^{dis}$ denote the upper limits of charging power and discharging power, respectively, while $\xi_{i,t}^{ch}$ and $\xi_{i,t}^{dis}$ indicate the charging and discharging states.

$$\begin{cases} 0 \le E \le E_{\max} \\ E_{i,t+1} = E_{i,t} - \Delta T \left(\dfrac{1}{\eta_t^{dis}} P_{i,t}^{dis} - \eta_t^{ch} P_{i,t}^{ch} \right) \\ E_{i,t} = ES_{i,t} \\ S_{\min} \le S_{i,t} \le S_{\max} \end{cases} \tag{6}$$

Equation (6) denotes the capacity constraints of MESSs, where $E_{\max}$ denotes the maximum capacity, η_t^{ch} and η_t^{dis} represent the charging and discharging coefficients, respectively, and $S_{\max}$ and $S_{\min}$ denote the upper and lower bounds of the state of charge (SOC).

$$\begin{cases} Zn_{ij,m,t} \le v_{\max} \Delta T \\ \sum_{m=1}^{M_c} \sum_{t=1}^{T} c_v Zn_{ij,m,t} \le C_{\max} \\ n_{ij,m,t} = \left| x_{m,t+1} - x_{m,t} \right| + \left| y_{m,t+1} - y_{m,t} \right| \end{cases} \tag{7}$$

In (7), the mobility process of MESSs is continued to be described in the manner of [15]. Where Z denotes the grid edge length; $n_{ij,m,t}$ represents the number of grid movements by the m^{th} MESSs at time t; M_c denotes the number of MESSs; $x_{m,t}$ and $y_{m,t}$ are decision variables indicating the position coordinates of the m^{th} MESS; $v_{\max}$ is the maximum operational speed of the MESSs; c_v represents the cost per unit distance of MESS; and $C_{\max}$ denotes the maximum available investment for planning energy storage mobility.

3) Network Constraints:

$$\begin{cases} \sum P_{i,t}^{in} + \xi_{i,t}^{dis} P_{i,t}^{dis} + P_{i,t}^{DG} = \sum P_{i,t}^{out} + \xi_{i,t}^{ch} P_{i,t}^{ch} + \sum_{i=1}^{N} x_{i,t} LD_{i,t} \\ -\alpha_{ij,t} P_{ij}^{\max} \le P_{ij,t} \le \alpha_{ij,t} P_{ij}^{\max} \\ -\alpha_{ij,t} Q_{ij}^{\max} \le Q_{ij,t} \le \alpha_{ij,l} Q_{ij}^{\max} \\ U_i^{\min} \le U_{i,t} \le U_i^{\max} \end{cases} \tag{8}$$

In (8), $P_{i,t}^{in}$ and $P_{i,t}^{out}$ denote the power flowing into and out of node *i*, respectively, while $\sum_{i=1}^{N} x_{i,t} LD_{i,t}$ represents the sum of all loads shed at node *i*. $P_{ij,t}$, $Q_{ij,t}$, and $U_{i,t}$ respectively represent the constraints on active power, reactive power, and voltage.

4) Additional Constraints:

$$\sum_{t=1}^{T-1} \left| x_{i,t+1} - x_{i,t} \right| \le X_{\max} \tag{9}$$

Where, $X_{\max}$ denotes the maximum number of switchings for a single bus node's load during a disaster period, serving as a constraint to avoid frequent switching.

$$\begin{cases} \xi_{i,t}^{l,ch} = 0 \\ \sum_{i=1}^{N_m} \xi_{i,t}^{l,ch} = 1 \\ \sum_{i=1}^{N_m} \xi_{i,t}^{l,dis} = 1 \end{cases} \tag{10}$$

Equation (10) indicates that MESS located at node *l,* which lacks DGs, cannot be charged. Furthermore, at most one MESS can perform charging or discharging at each node.

C. Dynamic frequency stability Constraints

Distribution network dynamic constraints primarily consider the imbalanced currents resulting from transmission line failures triggered by extreme weather conditions, which further induce frequency variations in the power system. Upon line disconnection, the power system segregates into two regions, with the inter-region swing equation given by (11):

$$\begin{cases} 2H_1 \dfrac{d\Delta f_1(t)}{dt} + D_1 \cdot P_1^D \cdot \Delta f_1(t) \\ \quad = PFR_1(t) - P_1^L + \Delta P_1^{\text{in}}(t) \\ 2H_2 \dfrac{d\Delta f_2(t)}{dt} + D_2 \cdot P_2^D \cdot \Delta f_2(t) \\ \quad = PFR_2(t) - P_2^L + \Delta P_2^{\text{in}}(t) \end{cases} \tag{11}$$

Where, H_1 and H_2 denote the inertia level of each region; $\Delta f_1(t)$ and $\Delta f_2(t)$ represent the frequency deviation in each

region; D_1 and P_1^D respectively denote the load damping coefficient and the size of the load in region 1; D_2 and P_2^D respectively denote the load damping coefficient and the size of the load in region 2; $PFR_1(t)$ and $PFR_2(t)$ indicates the primary frequency response capacity of each region; and $\Delta P_1^{\text{in}}(t)$ and $\Delta P_2^{\text{in}}(t)$ denote the power exchanged across inter-region tie lines following a power disturbance.

$$\Delta P_1^{in}(t) = \sum T_{1,2}\left[\int_0^t \Delta f_2(\tau)d\tau - \int_0^t \Delta f_1(\tau)d\tau\right] \tag{12}$$

$$T_{1,2} = 2\pi \cdot \frac{V_1 V_2}{X_{1,2}} \cdot \cos\left(\delta_1^{ss} - \delta_2^{ss}\right) \tag{13}$$

Where $T_{1,2}$ represents the electrical stiffness of the tie line, δ_1^{ss} and δ_2^{ss} denote the steady-state angular difference between the ends of the tie line, and $X_{1,2}$ indicates the transmission reactance of the tie line.

In [8], it has shown that in the event of a power shortfall within an electrical system, the process of frequency variation within any region can be characterized by changes in the Center of Inertia (COI) frequency, superimposed with oscillations between specific regions. Such oscillations diminish over time, thus primarily influencing the initial rate of frequency change and the frequency nadir value:

$$\Delta f_1(t) \approx \Delta f_{COI}(t) + e^{-at} A_1 \sin\left(\omega t + \phi_1\right) + C_1 \tag{14}$$

$$\begin{aligned}\Delta f_{COI}(t) = &\frac{2H_1R_1 + \left(D_1P_1^D + D_2P_2^D\right)T_d P^L}{\left(D_1P_1^D + D_2P_2^D\right)^2 T_d}\left(e^{-\frac{D't}{2H_1}} - 1\right) \\ &+ \frac{R_1 \cdot t}{\left(D_1P_1^D + D_2P_2^D\right)T_d}\end{aligned} \tag{15}$$

Where H denotes the inertia constants of each region; D represents the damping coefficient of the region; P denotes the total load of the region; R is the frequency regulation capacity, and T is the delivery time of frequency regulation capacity. Then, the constraints on ROCOF and frequency nadir can be derived and simplified in Section III.

III. Resilience Enhancement Model Solution

A. Handling Nonlinear Terms

In (5), due to the presence of nonlinear terms involving the product of 0-1 decision variables and continuous decision variables, denoted by $\xi_{i,t}^{dis} P_{i,t}^{dis}$ and $\xi_{i,t}^{ch} P_{i,t}^{ch}$, it is challenging to solve the model directly. By employing the Big-M method, decision variables μ_t are introduced to transform these terms, facilitating the solution of the model:

$$\begin{cases} 0 \le P_{i,t}^{ch} \le \mu_t P_{i,\max}^{ch} \\ 0 \le P_{i,t}^{dis} \le \left(1-\mu_t\right) P_{i,\max}^{dis} \end{cases} \tag{16}$$

Similarly, by introducing decision variables, (8) is simplified as:

$$\begin{cases} \sum P_{i,t}^{in} + K_1 + P_{i,t}^{DG} = \sum P_{i,t}^{out} + K_2 + K_3 \\ -M\left(1-\theta_1\right) \leqslant K_1 - P^{dis} \leqslant M\left(1-\theta_1\right), \quad 0 \leqslant K_1 \leqslant \theta_1 M \\ -M\left(1-\theta_2\right) \leqslant K_2 - P^{ch} \leqslant M\left(1-\theta_2\right), \quad 0 \leqslant K_2 \leqslant \theta_2 M \\ -M\left(1-\theta_3\right) \leqslant K_3 - LD \leqslant M\left(1-\theta_3\right), \quad 0 \leqslant K_3 \leqslant \theta_3 M \end{cases} \tag{17}$$

B. Linearization of Frequency Constraints

In [8] and [9], it has been demonstrated that ROCOF constraints and nadir constraints can be represented linearly.

1) ROCOF constraint:

ROCOF constraint for Region 1 is represented as follows:

$$\left|ROCOF_1\right| = \frac{P^L}{2\left(H_1 + H_2\right)} + A_1 \cdot \omega_1 \le ROCOF^{\max} \tag{18}$$

By employing numerical methods for parameter regression, a linearized form of the ROCOF constraint can be obtained:

$$\begin{aligned}\left|RoCoF_1\right| = &\frac{\Delta P^L}{2\left(H_1 + H_2\right)} + \frac{m_1H_1 + m_2D_1P_1^D + m_3R_1}{2\left(H_1 + H_2\right)} \\ &\frac{m_4H_2 + m_5D_2P_2^D + m_6R_6}{2\left(H_1 + H_2\right)} + \frac{m_7\Delta P^L + m_8}{2\left(H_1 + H_2\right)} \le RoCoF^{\max}\end{aligned} \tag{19}$$

Where m_1 to m_8 represent the parameters obtained through linear regression.

2) Nadir constraint:

Nadir constraint for Region 1 is represented as follows:

$$\begin{aligned}&\Delta P_1^L \cdot t_{nadir} \le 2H_1\Delta f_{Nadir}^{\max} + \frac{R_1}{T_d}\frac{\left(t_{nadir}\right)^2}{2} \\ &+ D_1P_1^D \int_0^{t_{nadir}} \Delta f_1(t)\mathrm{d}t + T_{1,2}\int_0^{t_{nadir}}\int_0^t \left[\Delta f_2(\tau) - \Delta f_1(\tau)\right]\mathrm{d}\tau\mathrm{d}t\end{aligned} \tag{20}$$

$$\begin{aligned}\int_0^{t_{nadir}} \Delta f_1(t) = &m_1'' H_1 + m_2'' H_2 + m_3'' \Delta P_1^L + m_4'' D_1 P_1^D \\ &+ m_5'' D_2 P_2^D + m_6'' R_1 + m_7'' R_2 + m_8''\end{aligned} \tag{21}$$

$$\begin{aligned}\int_0^{t_{nadir}}\int_0^t \left[\Delta f_2(\tau) - \Delta f_1(\tau)\right]d\tau dt = &m_1' H_1 + m_2' H_2 + m_3' \Delta P_1^L \\ &+ m_4' D_1 P_1^D + m_5' D_2 P_2^D + m_6' R_1 + m_7' R_2 + m_8'\end{aligned} \tag{22}$$

Wherein, $\Delta f_{Nadir}^{\max}$ is denoted as the frequency nadir; t_{nadir} represents the time it takes for the system frequency to reach its nadir, and it is necessary to achieve stable constraints by sampling and point selection within T_d; $\int_0^{t_{nadir}} \Delta f_1(t)\mathrm{d}t$ signifies the contribution of energy by the load damping in region 1, and $\int_0^{t_{nadir}}\int_0^t \left[\Delta f_2(\tau) - \Delta f_1(\tau)\right]d\tau dt$ denotes the energy transferred from region 2 to region 1. Moreover, these two can also be linearized through parameters obtained via linear regression.

Similarly, the ROCOF and nadir constraints for region 2 can be obtained through the same simplification method. Ultimately, constraints on the unbalanced power resulting from transmission line failures can be established, ensuring that the two independent microgrids formed post-fault remain in a frequency-stable state.

By extensively sampling and simulating the operating points of the power system, we obtain the corresponding values of the ROCOF and the lowest frequency points. Based on numerical regression, the linear representation coefficients are derived and incorporated into the optimization model as frequency stability constraints. Consequently, the entire model becomes a mixed-integer linear programming (MILP) model, facilitating the use of solvers for solution finding.

C. *Overall Solution Strategy*

The overall solution strategy for resilience enhancement under extreme weather conditions is shown in Fig. 2.

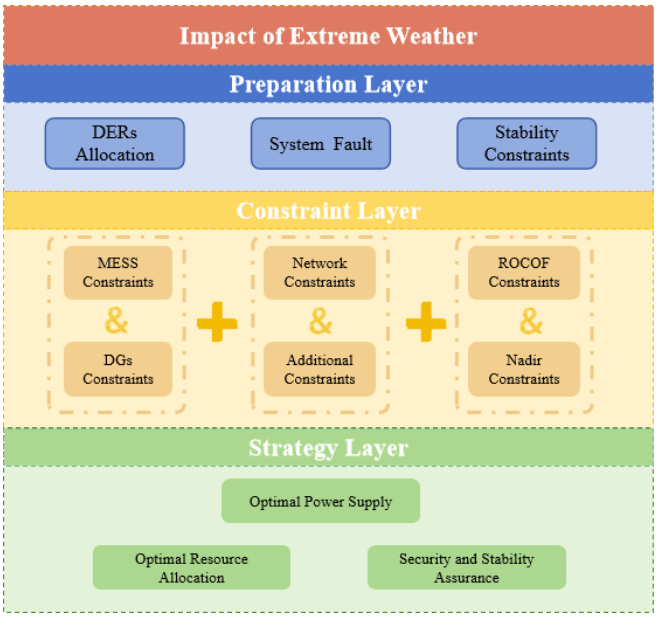

Fig. 2 . The overall solution strategy

IV. CASE STUDY

A. *Network Model and Parameter Settings*

This section of the study focuses on confirming the effectiveness of the suggested power grid resilience enhancement and resource allocation strategy through simulation experiments conducted using the IEEE 33-bus distribution system (as depicted in Fig. 3). The system undergoes a meshing process, with each mesh cell having a side length of 4km. The key parameters of the pre-set FERs for the simulation experiments are detailed in the TABLE I. and TABLE II. The unit configuration cost of MESS is 1300 ¥ / kW [16], with a maximum mobility speed of 80 km/s and charge efficiency η of 0.95. The cost of load shedding compensation is 10 ¥ / kW [17]. The frequency stability constraint $ROCOF^{\max}$ is set at 1 Hz/s, and $\Delta f_{Nadir}^{\max}$ is 0.8 Hz. The load damping coefficient D_L is 2%, and the frequency regulation capacity delivery time T_d is 10s[18].

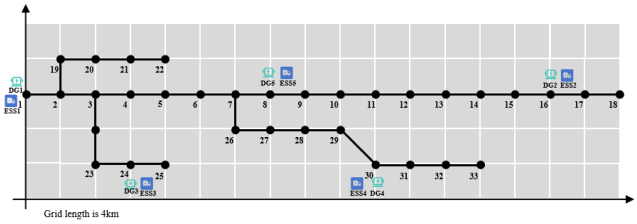

Fig. 3. IEEE 33-Bus Distribution System Network Topology Diagram

TABLE I. DG PARAMETERS

DG	Output Power Range (MW)	Ramping Capability Range(MW/h)	Node Location
DG1	[0.4, 8]	[-10, 10]	1
DG2	[0.4, 14]	[-3, 3]	16
DG3, DG4,DG5	[0.4, 8]	[-3, 3]	8,24,30

TABLE II. MESSS PARAMETERS

MESS	Output Power Range (MW)	SOC Range	Capacity Upper Limit (MW)	Node Location
MESS1,2 ,3,4,5	[-5, 5]	[0.1, 1]	10	1,8,16,24,30

It should be noted that extreme weathers and their impact on power grid faults have become the subject of research for many scholars and are not the focus of this paper[19][20]. Therefore, To rigorously validate the effectiveness of the proposed strategy, this study constructs a hypothetical scenario that encompasses a quintessential power system failure model, characterized by three transmission line faults occurring under extreme weather conditions (as detailed in TABLE III. and as depicted in Fig. 4). This scenario is engineered to enable a comprehensive analysis and critical evaluation of the strategy.

TABLE III. POWER SYSTEM FAULT INFORMATION

NO.	Faulty Line Location	Fault Time
Fault 1	13-14	T=2h
Fault 2	27-18	T=3h
Fault 3	4-5	T=4h

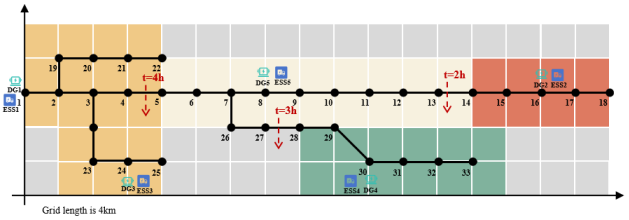

Fig. 4. Distribution Network System Under the Impact of Extreme Weather

B. *Economic Analysis of MESSs Allocation*

This subsection conducts a comparative analysis of the economic aspects of distributed resource allocation in enhancing the resilience of distribution networks through three methods. In Method 1, an optimized allocation strategy for MESSs is employed, disregarding dynamic frequency stability after faults

and focusing solely on static operational constraints before and after faults. In Method 2, the capacity allocation for each MESS is set to a fixed value. In Method 3, MESSs allocation is not considered; balance after faults is achieved solely through load shedding.

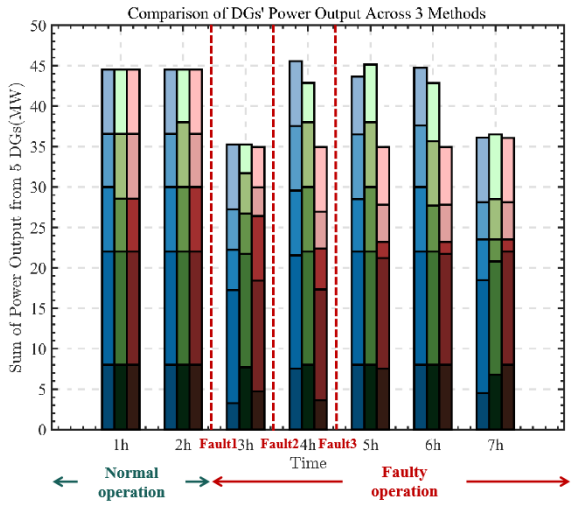

Fig. 5. Comparison of DGs' Power Output Across Three Methods

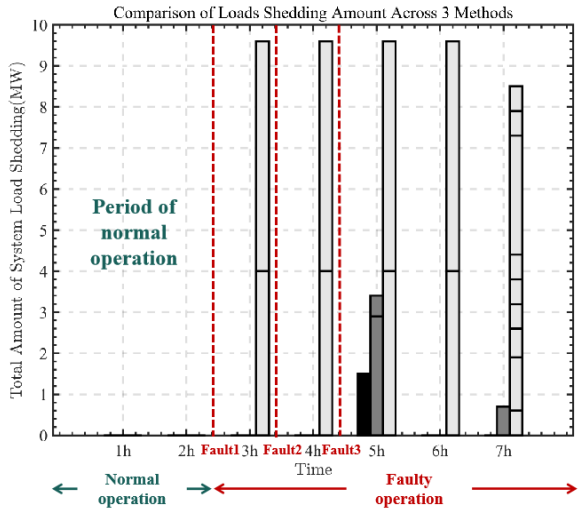

Fig. 6. Comparison of Loads Shedding Amount Across Three Methods

As depicted in Fig. 5, the blue, green, and red bar charts represent the power output of each PG (Power Generator) under method 1, 2, and 3, respectively, across different time periods. In Fig. 6, the bar chart colors, ranging from dark to light, represent the load shedding scenarios under different methods. Due to successive line faults in the distribution network system, it becomes challenging for local isolated networks to achieve local power supply-demand balance solely through DGs, necessitating load shedding. This is particularly the case when Fault 1 occurs between nodes 13-14, creating local Region 1 and Region 2. Given Region 2's limited supply scope, high demand, and the weaker support capability of DG2 within the region, Method 3, lacking MESSs for electrical support, requires significant load shedding. In contrast, Methods 1 and 2, with DER support, may only need minimal load shedding or even manage to fully guarantee power supply.

TABLE IV. ECONOMIC COMPARISON OF THE 3 METHODS

NO.	MESSs Capacity Allocation (MW)	MESSs Cost (¥)	Total Load Shedding Amount (MWh)	Resilience Index *R*	Total Cost (¥)
1	22.18	288360	1.5	15	304920
2	15	195000	15.35	633.5	829900
	22.18	228360	4.1	157	446930
	25	325000	2.4	24	350320
	35	455000	0	0	455880
3	0	0	46.9	2121	2121000

As shown in TABLE IV. , Method 3 results in a substantial amount of load shedding, failing to ensure widespread supply reliability and thus offering minimal economic value. The amount of load shedding in Method 2 is negatively correlated with the MESSs allocation capacity; however, its economic viability starts to significantly decrease once the allocation capacity surpasses a rational threshold. Method 1 balances both resilience and economic indicators, achieving an optimal allocation of FERs.

C. The Necessity of Considering Frequency Stability

This subsection conducts a comparative analysis through two methods on the necessity of considering dynamic frequency stability following power system faults in the process of enhancing resilience in distribution networks. Method 1 employs the resilience enhancement strategy with distributed resources under stable conditions proposed in this paper. In Method 2, dynamic frequency stability following faults is not considered, focusing solely on static operational constraints before and after the faults.

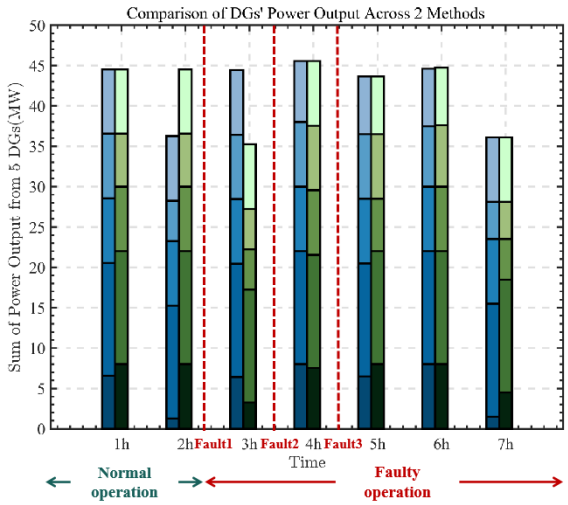

Fig. 7. Variations in DGs Power Output Across Two Methods

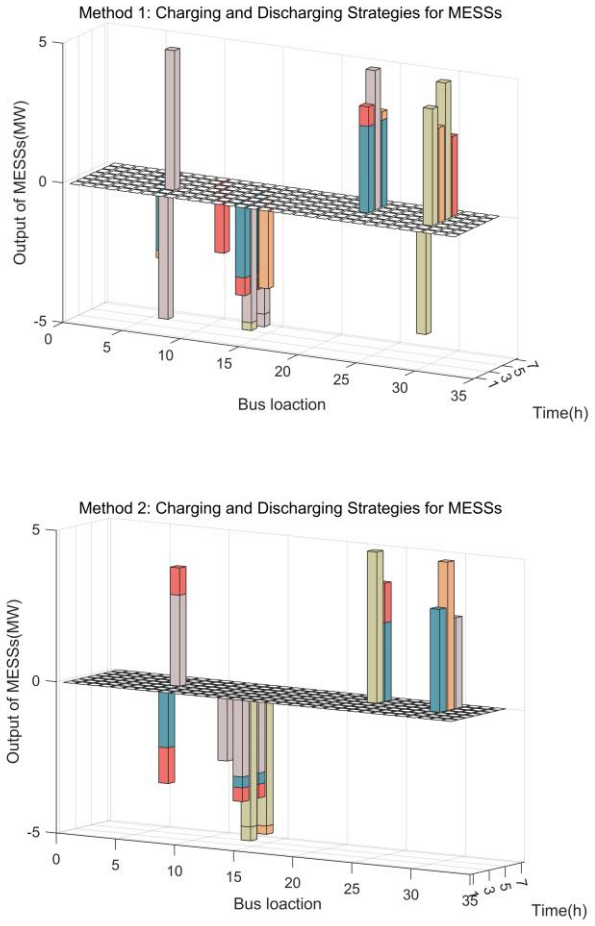

Fig. 8. Variations in Power Output of MESSs Across Two Methods

Fig. 7 and Fig. 8 illustrate the charging and discharging states of MESSs at different nodes and time periods. Method 1 exhibits a notable increase in the frequency of MESSs charging and discharging activities compared to Method 2, demonstrating a more proactive mobility strategy to support the needs of additional nodes. By conducting further optimization and scheduling of DGs and MESSs, Method 1 ensures that the impact on regional frequency due to unbalanced currents caused by line disconnections under extreme weather conditions is maintained within an acceptable range, as depicted in Fig. 9.

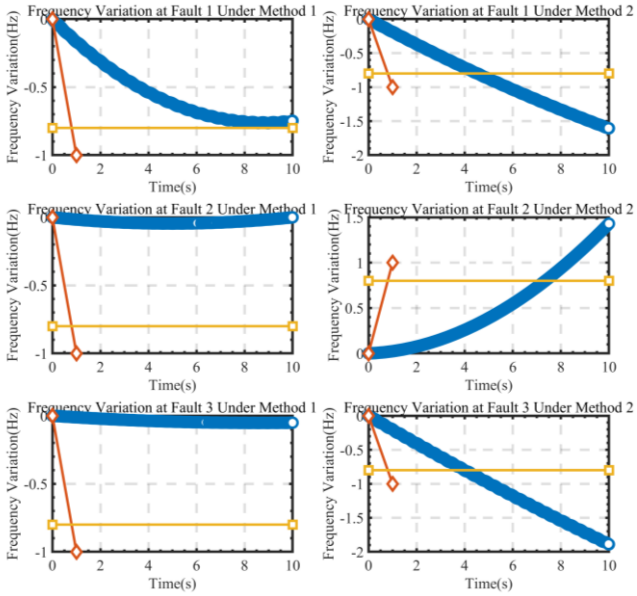

Fig. 9. Comparison of Frequency Variations Under Different Faults Across Two Methods

In Fig. 9, the blue curve represents the frequency variation curve of the fault area obtained through Simulink simulation. The red line indicates the maximum ROCOF during operation, and the yellow line represents the frequency nadir threshold allowed by the system. It illustrates that the resilience enhancement strategy implemented through Method 1, when facing Faults 1, 2, and 3, is capable of ensuring frequency stability across all regions, maintaining the nadir of frequency values above 49.2Hz, and keeping the ROCOF within 1Hz/s. In contrast, Method 2, by not considering frequency stability constraints, is susceptible to frequency deviations beyond safety limits under conditions of significant current imbalance, inadequate optimization of DGs, MESSs, and network flows, leading to severe safety risks. Therefore, Method 1 is more suited as a strategy for enhancing resilience.

V. Conclusion

This paper addresses the economic sustainability of FERs allocation under extreme weather conditions and the safety of frequency stability after faults occur. It proposes a resilience enhancement strategy for distribution network systems with FERs, incorporating regional frequency stability constraints. Initially, the paper extends beyond the conventional constraints on power output and capacity for DGs and MESSs by incorporating constraints specific to the location within the distribution network as well as constraints governing the mobility and charging/discharging locations of the ESS. Subsequently, employing numerical simulation techniques, it models the effect of unbalanced currents, resulting from line faults, on the frequency stability of isolated regions. The research linearizes the ROCOF and frequency nadir constraints to accurately characterize these aspects, ensuring their applicability in stability analysis. Ultimately, the study develops an optimized resource allocation and resilience enhancement strategy by considering the optimization of distributed resources in conjunction with frequency stability, aiming to bolster the system's safety and operational stability.

a)By gridifying the distribution network's nodes and lines, this paper achieves real-time constraints on the positions of MESSs. Taking into account the mobility speed of MESSs and the restrictions on charging/discharging locations, an optimization algorithm is employed to calculate the capacity allocation for each MESS. This is done to compensate nodes with insufficient DGs output in power system fault scenarios under extreme weather conditions. This method facilitates optimal resource allocation across the entire power grid, not only ensuring the resilience of the power system but also enhancing economic efficiency to the greatest extent possible.

b)By generating feasible operating points for the faulted area and conducting simulation simulations, regression analysis methods are employed to explore the boundaries of frequency stability. This approach yields linearized representation parameters for the ROCOF and the frequency nadir variations within the faulted area. These parameters are then integrated into the optimization process for resilience enhancement strategies. The results demonstrate that the method proposed in this paper can effectively ensure frequency stability in all areas during the dynamic process of faults.

It is noteworthy that the proposed strategy of configuring FERs with stability constraints under extreme weather conditions is applicable to most power system line fault situations. However, the formation of multi-regional independent power grids due to faults introduces more complex dynamic frequency stability constraints, increasing the computational requirements of the method. With the future integration of large-scale renewable resources, the power system's resilience may decline. Future research should explore the impact of renewable energy integration and changes in controllable loads on the optimization of FERs and frequency stability in modern power systems. Additionally, it should consider the aggregation and regulation of FERs in the grid to fully utilize their support advantages, aiming to further enhance the system's resilience to extreme weather events..

ACKNOWLEDGMENT

This work was supported by the Inner Mongolia Science and Technology Plan under Grant 2022JBGS0043.

REFERENCES

[1] State Grid Shanghai Electric Power: The grid line faults affected by Typhoon "Muifa" have been repaired. [Online]. Available: https://www.ndrc.gov.cn/fggz/jjyxtj/mdyqy/202209/t20220929_1337625.html.

[2] Southern Power Grid Battles "Soudelor": Full Power Restoration for Affected Users in Guangdong. [Online]. Available: http://www.sasac.gov.cn/n2588025/n2588119/c28783390/content.html.

[3] Y. Wang, Yin Xu, Jinghan He, Chen-Ching Liu, Kevin P. Schneider, et al., "Coordinating Multiple Sources for Service Restoration to Enhance Resilience of Distribution Systems," IEEE Transactions on Smart Grid, vol. 10, no. 5, pp. 5781–5793, Sep. 2019, doi: 10.1109/TSG.2019.2891515.

[4] WANG Zhenhao, LUO Jianxiao, CHENG Long, LI Guoqing, GU Xinran, "Improved graded load reduction strategy for resilience enhancement of an active distribution network in a typhoon," Power System Protection and Control, vol. 51, no. 22, pp. 34–48, 2023, doi: 10.19783/j.cnki.pspc.230233.

[5] PENG Jiasheng, WEN Yunfeng, LIANG Xiaorui, ZHANG Huaying, DONG Xin, YANG Youhang, "Resilience Coefficient Based Collaborative Optimization of Distribution Network Reconfiguration and Fault Repair," Automation of Electric Power Systems, pp. 1–13, doi:10.7500/AEPS20230330002.

[6] LI Minghao, YANG Qiming, LI Gengfeng, LIU Dafu, JI Chenlin, BIE Zhaohong, "Two-stage Power Supply Restoration Strategy of Resilient Distribution Network Based on Coordination of Multiple Distributed Resources in Typhoon Scenario," High Voltage Engineering, pp. 1–16, doi: 10.13336/j.1003-6520.hve.20231091.

[7] Y. Wang, D. Qiu, F. Teng, and G. Strbac, "Towards Microgrid Resilience Enhancement via Mobile Power Sources and Repair Crews: A Multi-Agent Reinforcement Learning Approach," IEEE Transactions on Power Systems, vol. 39, no. 1, pp. 1329–1345, Jan. 2024, doi: 10.1109/TPWRS.2023.3240479.

[8] L. Badesa, F. Teng, and G. Strbac, "Conditions for Regional Frequency Stability in Power System Scheduling—Part I: Theory," IEEE Transactions on Power Systems, vol. 36, no. 6, pp. 5558–5566, Nov. 2021, doi: 10.1109/TPWRS.2021.3073083.

[9] L. Badesa, F. Teng, and G. Strbac, "Conditions for Regional Frequency Stability in Power System Scheduling—Part II: Application to Unit Commitment," IEEE Transactions on Power Systems, vol. 36, no. 6, pp. 5567–5577, Nov. 2021, doi: 10.1109/TPWRS.2021.3073077.

[10] JIANG Yihang, ZHAO Shuqiang, WEI Ziyu, SUN Shuting, LI Zhiwei, "Distributionally Robust Unit Commitment Considering Regional Frequency Dynamic Differences and Whole Frequency Response Process," Proceedings of the CSEE, pp. 1–16.

[11] A. Vukojevic and S. Lukic, "Microgrid Protection and Control Schemes for Seamless Transition to Island and Grid Synchronization," IEEE Trans. Smart Grid, vol. 11, no. 4, pp. 2845-2855, July 2020, doi: 10.1109/TSG.2020.2975850.

[12] A. M. Nakiganda, S. Dehghan, U. Markovic, G. Hug, and P. Aristidou, "A Stochastic-Robust Approach for Resilient Microgrid Investment Planning Under Static and Transient Islanding Security Constraints," IEEE Trans. Smart Grid, vol. 13, no. 3, pp. 1774–1788, May 2022, doi: 10.1109/TSG.2022.3146193.

[13] WU Yiwei, LIM G J, SHI Jian. "Stability-constrained microgrid operation scheduling incorporating frequency control reserve". IEEE Transactions on Smart Grid, 2020, 11(2): 1007-1017.

[14] BIE Zhaohong, LIN Yanling, QIU Aici. "Concept and Research Prospects of Power System Resilience." Automation of Electric Power Systems 39.22(2015):1-9. doi:CNKI:SUN:DLXT.0.2015-22-001.

[15] WANG Yushan, DENG Hui, WANG Xu, JIANG Chuanœen, FANG Le, MA Junchao. "Optimal Configuration and Operation Strategy of Mobile Energy Storage in Distribution Network Considering Spatial-Temporal Evolution of Typhoon". Automation of Electric Power Systems, 2022, 46(9): 42-51.

[16] SUN Yunzhi, JIANG Deyu, ZHANG Shenglin, LIANG Rong, LI Peidong, et al. "Optimal configuration of multi-energy microgrid energy storage considering battery life loss". Journal of Electric Power System and Automation. 2021,33(5):128-133.

[17] ZOU Bo, SUN Ke, HU Chengpeng, et al. "Strategy for resilience improvement of distribution system under typhoon weather". Journal of Electric Power System and Automation, 2021,33（7）:135-142.

[18] F. Teng, V. Trovato, and G. Strbac, "Stochastic Scheduling With Inertia-Dependent Fast Frequency Response Requirements," IEEE Transactions on Power Systems, vol. 31, no. 2, pp. 1557–1566, Mar. 2016, doi: 10.1109/TPWRS.2015.2434837.

[19] WANG Zhenhao, LUO Jianxiao, CHENG Long, LI Guoqing, GU Xinran, et al."Improved graded load reduction strategy for resilience enhancement of an active distribution network in a typhoon." Power System Protection and Control 51.22(2023):34-48. doi:10.19783/j.cnki.pspc.230233.

[20] Y. Tao, J. Qiu, S. Lai, X. Sun and J. Zhao, "Vulnerability Assessment of Coupled Transportation and Multi-Energy Networks Considering Electric and Hydrogen Vehicles," in IEEE Transactions on Intelligent Transportation Systems, vol. 24, no. 11, pp. 12614-12626, Nov. 2023, doi: 10.1109/TITS.2023.3287529.